Rational design of SiBCN microstructures using direct photolithography of patternable preceramic photoresists

Quentin Hanniet, Eddy Petit, Sylvie Calas-Etienne, Pascal Etienne, Karim Aissou, Benoit Charlot, Christel Gervais, P. Miele, Chrystelle Salameh

Materials & Design 223 (2022) 111234

Contents lists available at ScienceDirect

Materials & Design

journal homepage: www.elsevier.com/locate/matdes

Rational design of SiBCN microstructures using direct photolithography of patternable preceramic photoresists

Quentin Hanniet [a], Eddy Petit [a], Sylvie Calas-Etienne [b], Pascal Etienne [b], Karim Aissou [a], Christel Gervais [c], Philippe Miele [a], Benoit Charlot [d], Chrystelle Salameh [a,*]

[a] Institut Européen des Membranes, IEM, UMR 5635, Univ Montpellier, ENSCM, CNRS, Montpellier, France
[b] Laboratoire Charles Coulomb, UMR 5221 CNRS, Université de Montpellier, 34095 Montpellier, France
[c] Sorbonne Université, UMR 7574 CNRS, Laboratoire de Chimie de la Matière Condensée de Paris, LCMCP, F-75005 Paris, France
[d] Institut d'Électronique et des Systèmes, UMR 5214 CNRS, University of Montpellier, Montpellier, France

HIGHLIGHTS

- Crack-free SiBCN microparts (20–200 μm) are obtained by direct photolithography of molecularly designed boron-containing photocurable preceramic polymers.
- Surface roughness below 3 nm and Young's modulus of ~ 60 GPa attest the high quality of SiBCN patterns and pave the way to applications in microfabrication and microfluidics.

GRAPHICAL ABSTRACT

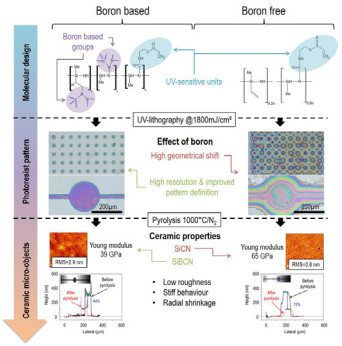

ARTICLE INFO

Article history:
Received 10 May 2022
Revised 10 September 2022
Accepted 4 October 2022
Available online 5 October 2022

Keywords:
Preceramic photoresists
SiBCN
Photolithography
MEMS

ABSTRACT

Non-oxide ceramic MEMS based on Si, C, N and B elements are of great importance for high-temperature applications in harsh and oxidizing conditions including electronics, photonics and actuators. Yet, structuring and patterning ceramics is challenging and often relies on conventional soft-lithography or molding processes that can introduce defects and cracks leading to a decrease in the device's performance. Herein, we report on the design for the first time of SiBCN ceramic micro-components (in the 20–200 μm range) from direct patterning of "tailor-made" UV-curable boron-modified polyvinylsilazane preceramic (polyborovinylsilazane) resins. This approach first involves a two-step chemical synthesis of patternable preceramic polymers through acrylate or methacrylate grafting onto polyborovinylsilazane followed by subsequent crosslinking under UV light. FTIR and NMR spectroscopies confirmed the successful grafting of boron and photocurable units on the preceramic polymers while thermogravimetric analysis was used to monitor the polymer-to-ceramic conversion. SiBCN micro-objects obtained after pyrolysis were thoroughly characterized by SEM, AFM, nanoindentation and profilometry techniques. The Young's modulus results for such microstructures (~60 GPa) are characteristic of good mechanical properties making these ceramic microstructures promising materials for MEMS applications.

* Corresponding author.
E-mail addresses: chrystelle.salameh@umontpellier.fr, chrystelle.salameh@enscm.fr (C. Salameh).

https://doi.org/10.1016/j.matdes.2022.111234
0264-1275/

1. Introduction

In the last few years, micro- and nano-electrochemical systems (MEMS/NEMS) have been extensively studied due to their potential applications in the fields of micro/nanofluidics, photonics, electronics and actuators [1,2,3]. One of the important research axes of this field of study is the development of MEMS/NEMS based on innovative and customized materials [4,5,6]. While conventional MEMS and NEMS may lack thermal and chemical stability in severe environments, ceramics are recognized as the most durable materials for fabricating highly stable advanced micro-components. The traditional ceramic process (*i.e.* shaping of ceramic parts from powder) remains however hardly compatible with the preparation of MEMS and NEMS given the size and complexity of the shapes sought. The high chemical, mechanical and thermal resistance of silicon-based ceramics, in particular for non-oxide compositions, represent great potential for MEMS [7,8,9,10]. In this context, several techniques have been developed to combine microfabrication with ceramic design, including Si-micromachining, Low & High-Temperature Co-firing Ceramics (LTCC and HTCC), Chemical Vapor Deposition (CVD) and Physical Vapor Deposition (PVD) [11,12,13,14,1819]. Nevertheless, these techniques are limited by their high cost, time-consuming aspect and inability to produce precise and fine complex shapes. The Polymer-Derived Ceramics (PDCs) route, consisting in the conversion of polymer precursors into inert amorphous ceramics, is particularly suitable for elaboration of complex-shaped MEMS and micro-objects [20,15,16,17]. Indeed, the structure and properties of the final ceramic can be adjusted by designing at molecular level the precursor's chemistry. Soft-lithography and photolithography are two fabrication techniques widely used for micro-shaping and can be adapted to preceramic polymers *via* elastomeric mold or UV-lithography, respectively [22–26]. Soft-lithography involves initial preparation of microstructures on a duroplastic polymer like polydimethylsiloxane (PDMS) followed by molding or printing. Direct lithography consists in structuring crosslinkable preceramic polymers using energy sources such as ultraviolet (UV), electron beam (E beam), laser or X-ray. Since early 2000′s, few reports on soft-lithography techniques coupled with the PDCs technique concerned the preparation of SiC [27] SiOC [28,29], SiCN [30–32], and SiBCN [33] micro-parts. Schulz's review gives a wide description of potential applications and possibilities given by the PDCs route when combined with lithography methods [34]. Photolithography is generally preferred to soft-lithography thanks to the rapid and selective UV-curing that avoids the steps of mold preparation, molding and demolding. Therefore, interest in preparing preceramic photoresists has significantly increased. Indeed one of the advantages of the PDCs process is the possibility to tune specific properties through chemical modification of the preceramic polymer. Several works described the grafting of photocurable functions onto preceramic polymers thus initiating direct patterning of the material through UV crosslinking. PDCs micro-patterning prepared from acrylated or methacrylated preceramic negative photoresists is a strategy already reported in the literature, in particular for SiCN [35–42] or SiOC [43] micro-objects. On the other hand, SiC patterning resulting from micro-stereolithography can be carried out without grafting any photocurable function on the polymer backbone [44]. However, to the best of our knowledge, direct lithography of more complex quaternary systems such as SiBCN exhibiting superior high temperature stability has not been reported yet. Chemical modification of commercial preceramic polymers such as polycarbosilane, polysilazane or polysiloxane can lead to novel ceramic materials. For example, the introduction of a new element X (X = Al, B, Fe…) during the synthesis step will conduct to a Si-X-(O)-C-(N) amorphous ceramic with specific properties. Si-Fe—C—N [45], Si-Al—C—N [46], Si-B—C—N [47–50], and other multi-components ceramics were recently described in the literature. In particular, introducing boron in SiCN matrix leads to an amorphous microstructure composed of SiC, Si_3N_4, BN and free carbon nanodomains, particularly stable at high temperature and resistant to the crystallization process [51,52]. Developing advanced and cost-effective approaches to design materials with desired shapes and properties has always been a prime focus of materials research. In this work, we report on the synthesis of UV-curable polyborovinylsilazane photoresists and we describe their patterning by direct photolithography. A commercial polyvinylsilazane was first modified by boron through dehydrocoupling and/or hydroboration of vinyl and/or N—H functions, respectively. Photocurable acrylate or methacrylate units were then grafted onto the polyborovinylsilazane by adding isocyanate on N—H functions for the production of SiBCN ceramic micropatterns. Full chemical characterization of these original preceramic photoresists was carried out through Fourier-Transform InfraRed spectroscopy (FTIR), Nuclear Magnetic Resonance spectroscopy (NMR) and ThermoGravimetric Analysis (TGA). The influence of the quantity of boron and photocurable functions on the UV absorption and ceramic yield was evaluated. SiCN and SiBCN micropatterns derived from the synthesized photoresists were obtained *via* photolithography process followed by pyrolysis and were characterized by Scanning Electron Microscopy (SEM), Atomic Force Microscopy (AFM) and profilometry. The mechanical resistance of the ceramic micropatterns was measured by nanoindentation. As far as we know the synthesis of such SiBCN precursor photoresist and such an extensive study has not been reported in the literature. This approach could be extended to other non-oxide ceramics in which composition and microstructure can be tuned to control the quality and properties of the material. More generally, these results extend the compositional panel of the ceramics used for MEMS opening interesting perpectives in terms of research on ceramics applied to several branches of technology.

2. Materials & methods

2.1. Reagents and chemicals

Durazane 1800 (Polyvinylsilazane PVZ) –commercial precursor of SiCN ceramic – was purchased from Merck, Darmstadt, Germany. Borane dimethylsulfide complex (BDMS, 2 M in toluene, Alfa Asear, Kandel, Germany) and toluene (anhydrous 99.8 %, Merck, Darmstadt, Germany) were used as received under argon flow for the preparation of Polyborovinylsilazane (PBVZ). Isocyanatoethyl methacrylate (IEM) and Isocyanatoethyl acrylate (IEA) were provided by ABCR (Karlsruhe, Germany) and used as received for the grafting of acrylate and methacrylate functions on P(B)VZ. 2-Benzyl-2-dimethylamino-1-(4-morpholinophenyl)-butanone-1 from ABCR (Karlsruhe, Germany) (BDMB) was used as Norrish photoinitiator for UV crosslinking.

2.2. Synthesis of the preceramic photoresists

The synthesis of polyborovinylsilazane PBVZ was carried out under argon atmosphere using a Schlenk line. In a typical synthesis, 100 mL of toluene and 5 g of PVZ were added to a three-neck round-bottom flask under argon flow. The BDMS solution was slowly introduced at 0 °C to the mixture *via* an addition funnel (2.4 mL for Si/B = 17 ratio and 1.3 mL for Si/B = 30 ratio). The Si/B ratio of 17 corresponds to the BDMS quantity required for a complete hydroboration of the vinyl units in PVZ and it conducts to a highly viscous liquid suggesting a high crosslinking rate. As for Si/B = 30, a partial hydroboration of vinyl units occurs giving a less

viscous solution of PBVZ. After complete addition of BDMS, the mixture was kept under stirring for 72 h at room temperature. The toluene was then removed by distillation at reduced pressure, yielding a viscous translucent solution of PBVZ polymer. The grafting of acrylate and methacrylate was carried out after the introduction of boron in the preceramic polymer in the case of PBVZ. Typically, in a three-neck round-bottom flask 5 g of P(B)VZ was dissolved in 100 mL of toluene. 10 wt% of IEA (or IEM) was introduced dropwise to a certain amount of P(B)VZ (500 mg in this example) and the mixture was left at room temperature overnight under vigorous stirring. After solvent removal, the final product was recovered under argon inside a LABstar pro, Mbraun glove box. Table SI 1 summarizes the synthesis parameters of the different preceramic photoresists prepared in this study.

2.3. Fabrication of Si(B)CN microcomponents

Fig. SI 1 represents the top-down photolithography process used for the preparation of SiCN and SiBCN micropatterns. The photoresist solutions were prepared by dissolving preceramic polymers (polysilazane or polyborosilazane) in toluene at 50 mg/mL with 3 wt% of BDMB. Thin film of preceramic polymer was prepared by spin coating of the negative photoresist solution at 1000 rpm for 30 s and 2000 rpm for 10 s. Photolithographic mask (~20–200 μm dimensions) was then applied on the film surface and UV irradiation was performed from 10 to 90 s (100 W; 365 nm; mercury bulb; UVP Blak-ray series) to selectively crosslink specific areas of the thin film. Microscopy observation of the photomask layout is available in supporting information (Fig. SI 2). Unreacted preceramic photoresist was removed by developing the thin film in ethanol for 20 s then rinsed with acetone. Preceramic micropatterns were introduced in a tubular furnace (type ROS20/250/12 with a silica tube, Thermconcept, Bremen, Germany) and slowly heated at 1000 °C for 2 h under nitrogen atmosphere (heating rate 1 °C/min; cooling rate 2 °C/min).

2.4. Characterization of the preceramic photoresists

Polymer-to-ceramic conversion was monitored by thermogravimetric analysis (TGA), using a TGA-STD Q600 thermal analysis device, from RT up to 1000 °C at 5 °C/min in nitrogen atmosphere (100 mL/min flow). The chemical structure of the preceramic polymers was investigated by Fourier Transform InfraRed (FT-IR) spectroscopy with a Nexus IS-50 Thermo scientific spectrometer using KBr pellets (2 wt% of polymer mixed with previously dried KBr powder followed by compaction into a dense pellet). ^{1}H, ^{13}C and ^{29}Si Nuclear Magnetic Resonance (NMR) spectroscopy was also performed on the samples dissolved in deuterated THF and analysed with a Bruker AM 300 spectrometer operated at 300 MHz. Chemical characterization was completed by diffusion-ordered NMR spectroscopy (DOSY) carried out with a Bruker Avance III 600 spectrometer operating at 600 MHz and equipped with a probe Prodigy TCI. DOSY data set is typically acquired using a pulsed field gradient spin echo or stimulated echo (PFGSE or PFGSTE) pulse sequence. Diffusion information is obtained by recording spectra with different field gradient pulse amplitudes. A diffusion coefficient for each signal can be obtained by fitting the signal attenuation to the equation ***Eq1*** for unrestricted diffusion.

$$\rho = \exp[-D(\gamma g \delta)^2\left(\Delta - \frac{\delta}{3}\right)] \quad (1)$$

where $\boldsymbol{\rho}$ is the Attenuation Factor, $\boldsymbol{D}$ is the diffusion coefficient, γ is the magnetogyric ratio, $\boldsymbol{g}$ is the gradient strength, Δ is the corrected diffusion time and δ is the gradient pulse width.

Solid-state ^{29}Si MAS and ^{13}C CP MAS NMR were recorded on a Bruker Avance 300 spectrometer (B_0 = 7.0 T, ν_0 (^{1}H) = 300.29 MH z, ν_0 (^{13}C) = 75.51 MHz, ν_0 (^{29}Si) = 59.66 MHz) and 700 spectrometers (B_0 = 16.3 T, ν_0 (^{1}H) = 699.97 MHz, ν_0 (^{13}C) = 176.02 MHz) using a 4 mm Bruker probe and spinning frequency of 10 kHz. The chemical shift values were referenced to TMS for ^{13}C and ^{29}Si. The photosensitivity of the synthesized polymers was evaluated by UltraViolet–visible spectroscopy. UV absorbance spectra were recorded on a JASCO V-570 spectrometer on 200–450 nm wavelength range. Analysed products were dissolved in THF (0.5 mg/mL) and placed in quartz cells.

2.5. Characterization of the ceramic micropatterns

Morphology and elemental composition of the prepared micropatterns were investigated by Scanning Electron Microscopy (SEM) and Energy Dispersive X-ray analysis (EDX). Samples were Platinum metalized and observed with a Hitachi S4800 SEM. High-resolution pictures of the micropatterns were generated by a Keyence VHX-7000 numerical microscope. Atomic force microscopy (AFM Nano-Observer, CSInstruments) was used in tapping mode to characterize the top surface morphology as well as the profile of the SiBCN micropatterns. Silicon cantilevers (PPP-NCH, Nanosensors) with a typical tip radius of ~ 5 nm were used. The resonance frequency of the cantilever was about 235 kHz. The profilometry investigation of the samples was carried out using a Veeco Dektak 150 profiler (Veeco, Plainview, NY, USA). Nanoindentation experiments were performed using CSM Instruments Open Platforms. Indentations are conducted using a Berkovitch indentor (pyramidal tip). Indentation sites are selected by optic microscopy (x500). The load range is from 10 μN to 500 μN (resolution 0.1 μN and 0.1 nm) for the ultra nanoindentation platform. The force required to indent the material is monitored as a function of the penetration depth. The elastic modulus of the samples can be derived from the load–displacement loading/unloading curves. The data are analyzed with the most extensively used method proposed by Oliver and Pharr [53].

3. Results and discussion

3.1. Characterization of the preceramic photoresists

3.1.1. FTIR spectroscopy

Mechanisms describing the incorporation of boron into polyvinylsilazane by dehydrocoupling and hydroboration are presented in Fig. SI 3 and Fig. SI 4, respectively. Dehydrocoupling between N—H functions of PVZ and B-H of BDMS forms B-N bonds leading to crosslinking of the polymer. Hydroboration of the vinyl functions in PVZ by BDMS corresponds to the formation of B-C bond. PBVZ17 and PBVZ30 polymers with Si/B = 17 and Si/B = 30 ratios, respectively, were synthesized. FTIR spectra corresponding to the as-synthesized polymers are presented in Fig. 1. Characteristic units of PVZ (Fig. 1.a, black line) are detected at 2126, 3400, 1253 and 1166 cm^{-1} and correspond to Si-H stretching, ≡Si—N—H stretching, deformation of CH in Si-CH_3, and Si-N vibration bands, respectively. Presence of the vinyl group is confirmed by the C=C stretching, the CH_x deformation in the vinyl function and the CH stretching bands at 1593, 1400 and 3047/3005 cm^{-1} respectively. Bands below 1000 cm^{-1} are hardly distinguishable because of the overlap but Si-C around 850 cm^{-1} and Si-N around 700 cm^{-1} can be isolated. Similarly, PBVZ30 spectrum (Fig. 1.b, burgundy line) presents the same bands of PVZ with a reduced intensity of CH stretching bands at 3047 and 3005 cm^{-1} and Si-CH = CH_2 band at 1593 cm^{-1}. The consumption of the vinyl group is probably associated with the hydroboration of the vinyl functions by BDMS.

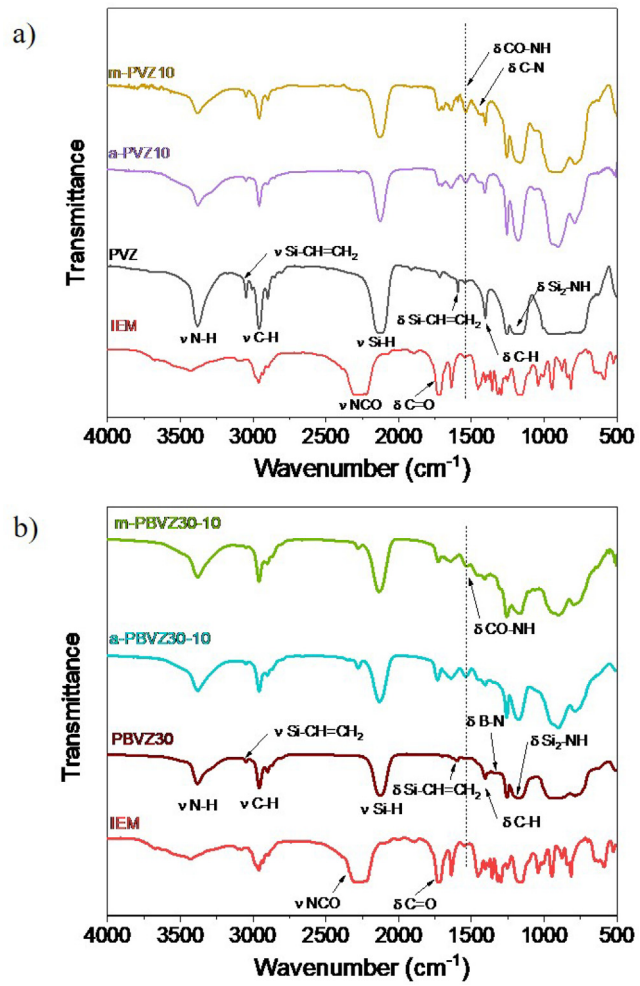

Fig. 1. FTIR spectra: a) Boron-free photoresist aPVZ10 and mPVZ10 b) Boron-based photoresist with ratio Si/B = 30.

Similar conclusions can be made for PBVZ17 (Fig. SI 5, blue line) but in addition, the B-N band detected around 1300 cm^{-1} confirms the dehydrocoupling reaction between N—H and B-H groups. Moreover, B-H band around 2400 cm^{-1} can be distinguished and suggests that BDMS is not completely consumed during the synthesis of PBVZ17. The grafting of acrylate and methacrylate functions on PVZ and PBVZ (see mechanisms in Fig. SI 6 and Fig. SI 7 in Supporting Information) was monitored by FTIR analysis, results are presented in Fig. 1 and Fig. SI 5. Photocurable entities are grafted onto the polyvinylsilazane backbone *via* the addition of isocyanate functions (-NCO) to N—H groups to form urea bonds (–CO-NH-). This reaction is confirmed by the appearance of an absorption peak assigned to the urea group at 1545 cm^{-1} [37]. The nearly disappearance of the isocyanate peaks (–NCO) at 2272 and 1363 cm^{-1} confirms the consumption of the function to form urea. Further, the signals of incorporated methacrylate or acrylate functions appear at 1714 cm^{-1} (C=O) and 1639 cm^{-1} (C=C). According to FTIR, the grafting of acrylate or methacrylate on PBVZ and PVZ is confirmed. Nevertheless, NMR characterization of preceramic photoresists was also performed to obtain a better description of the molecular structure.

3.1.2. NMR spectroscopy

Fig. SI 8.a and SI 8.b display the ^{1}H NMR spectra and DOSY (Diffusion Ordered SpectroscopY NMR) analysis associated with PVZ, aPVZ10 and mPVZ10, respectively. Discussion and interpretation of these figures are available in supporting information. ^{1}H NMR analyzes of boron based photosensitive resins are presented in Fig. 2.a. The characteristic chemical functions of PVZ are found in PBVZ30 with nevertheless a decrease in the intensity of the signal associated with Si-CH = C**H**$_2$ (5.9–6.3 ppm) probably caused by hydroboration *via* BDMS (see mechanism in Fig. SI 4). After the addition of IEA or IEM, C**H**$_2$-NH and C**H**$_2$-O groups are visible but with a much weaker intensity than in the case of boron-free resists. This suggests that the grafting of the photosensitive groups is less favorable in the presence of boron, which is consistent with the FTIR analyzes presented in Fig. 1. The steric hindrance and the consumption of a part of the N—H groups caused by the dehydrocoupling reactions, taking place during the introduction of boron (see Fig. SI 3), can reduce the availability of N—H sites for the grafting of the acrylate/methacrylate groups. Despite the low intensity of the signals associated with the photosensitive groups, the DOSY analysis (Fig. 2b) confirms the successful grafting of the photosensitive units on the polymer chain with a Brownian motion mode around $10^{-9.5}$ m^2/s. The NMR study is finally completed with solid-state NMR (Fig SI 9) carried out on crosslinked samples.

3.1.3. Thermogravimetric analysis

Fig. 3.a and 3.b show the TGA curves under nitrogen atmosphere of PVZ and PBVZ photoresists, respectively. The degradation of PVZ occurs in 3 steps: a first massive weight loss between 100 °C and 250 °C is attributed to the evacuation of gaseous NH_3 and small oligomers; a second weight loss between 300 and 500 °C corresponds to the release of C_xH_y species (with 2 to 4 carbons) and a final decomposition between 600 and 1000 °C is associated with the ceramization of preceramic polymers by release of CH_4, and H_2 [49]. Introduction of acrylate and methacrylate functions increases the ceramic yield of modified PVZ (67 % for aPVZ20 and

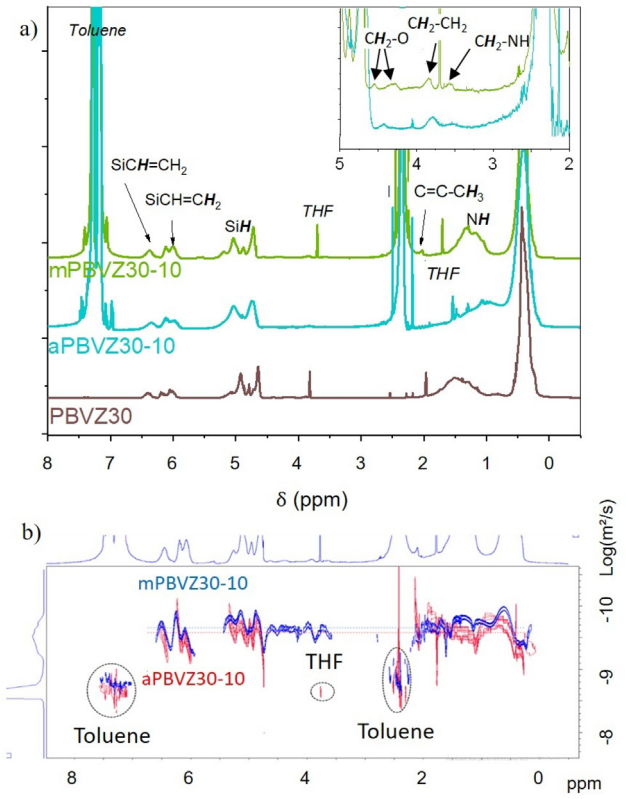

Fig. 2. a) ^{1}H NMR spectroscopy of PBVZ30, aPBVZ30-10 and mPVZ30-10 (small scope in inset) and a) 2D DOSY analysis for aPBVZ30-10 and mPVZ30-10; 50 mg/ml in deuterated THF.

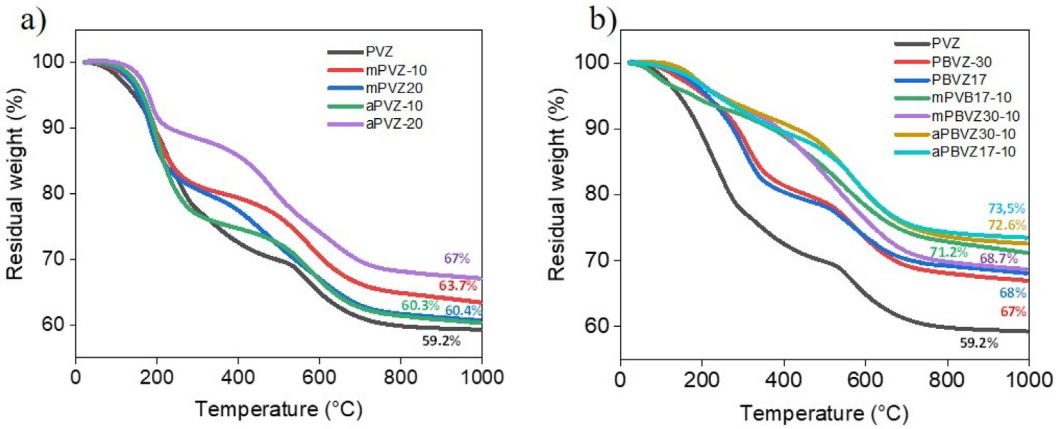

Fig. 3. TGA curves under nitrogen a) preceramic polymers without boron b) preceramic polymers with boron.

61 % for mPVZ20 *versus* 59 % for PVZ). This can be explained by an early crosslinking of the polymer initiated by the grafting of IEA or IEM as evidenced by the increase of the viscosity during the synthesis. Furthermore, the degree of crosslinking seems higher for samples modified with 10 % methacrylate than for samples modified with acrylate, which justifies the higher weight loss measured for aPVZ10 against mPVZ10. Addition of boron clearly increases the ceramic yield of the preceramic polymer to approximately 67 % for Si/B = 30 and 68 % for Si/B = 17. For polymers containing boron, the first weight loss (from 150 to 250 °C) is reduced compared to PVZ. Indeed, a certain amount of vinyl and N—H groups were consumed during the synthesis of PBVZ by the formation of B-N and B-C bonds (see mechanisms in Figs. SI 3 and SI 4). Under these conditions, transamination reactions leading to the release of NH_3 are less likely to occur. Finally, the high ceramic yield of PBVZ photoresists can be explained by the grafting of acrylate/methacrylate (ceramic yield reaches almost 75 % for aPBVZ17-10). Strong shrinkage occurs during pyrolysis, which can lead to "mud-cracks" or other defects [54,55]. Increasing the ceramic yield of the photoresist is of great importance as it generally limits the shrinkage upon pyrolysis.

3.2. Characterization of the ceramic micropatterns

3.2.1. Morphological properties

3.2.1.1. Before pyrolysis. Optimization of the photolithography process is necessary to obtain the most faithful reproduction of the pattern of the lithographic mask. The dose-to-size (E_s) value corresponds to the amount of energy exposure required to produce the proper dimension of the resist feature [56]. The evaluation of E_s of each of the synthesized preceramic photoresists was performed through a UV-dose test. It consists in exposing the spin-coated photoresist film with different amounts of irradiation energy. After development, the obtained micropatterns were observed with high-resolution numerical microscopy as shown in Fig. 4 and in supporting information (Fig SI 11 to SI 13). Four areas are visible on the micrographs and correspond to UV exposure of 10, 30, 60 and 90 s with a 365 nm UV lamp. As the delivered intensity of the lamp is 20 mW/cm^2, the densities of energy irradiating the 4 areas are 200; 600; 1200 and 1800 mJ/cm^2, respectively. The lithographic mask micrographs in Fig. SI 2 displays the pattern dimensions and shape. They reveal 4 different models A, B, C and D corresponding to small dots with radius R_s, big dots with radius R_b, big channels with W_b width and small channels with radius R_c and width W_c, respectively. The UV dose tests presented in Fig. 4.a and SI 13 correspond to aPBVZ30-10 and mPBVZ30-10 photoresists, respectively. For an exposure time of 10 s (200 mJ/cm^2), the exposed polymer is completely dissolved after the development step, no micropatterns are visible for the two photoresists. For an exposure of 30 and 60 s (600 and 1200 mJ/cm^2), some micropatterns are visible but the reproduction of the mask pattern is not accurate. For a 30 s exposure, small dots (pattern A), large dots (pattern B) and small channels (pattern D) are smaller than expected (radius and channel shift between 5 and 9 μm) in the case of aPBVZ30-10 and almost missing for mPBVZ30-10. Mask pattern reproduction is more accurate for a 60 s exposure but models B and D are damaged by the development step. In conclusion, the most faithful reproduction for the two photoresists is obtained for an energy density energy of 1800 mJ/cm^2 with undamaged patterns and an overpolymerization below 12 μm. The aPBVZ30-10 resist displays high resolution as shown by the well defined 20 μm dot grid made with 1800 mJ/cm^2. For comparison, a recently developed acrylic resin reveals a similar resolution ~ 20 μm [57]. Nevertheless, in the case of mPBVZ30-10, the small dots of pattern A are absent unlike sample aPBVZ30-10. This is relevant with the lower reactivity of methacrylate functions compared to acrylate as mentioned previously. In summary, aPBVZ30-10 and mPBVZ30-10 photoresists seem to be ideally crosslinked by an irradiation energy density between 1200 and 1800 mJ/cm^2. Additionally, the presence of boron in the photoresist decreases the reactivity of aPBVZ30-10 and mPBVZ30-10 to UV light compared to boron-free photoresists. This is consistent with the NMR analysis in Fig. 2 showing that the grafting of photosensitive units is less likely to occur in presence of boron in the polymer. The lower amount of acrylate/methacrylate groups leads to a lower photosensitivity of photoresists containing boron. Similar UV-dose tests were carried out on boron-free photoresists, there discussion, interpretation and micrographs are displayed in supporting information (Fig. SI 11 and SI 12).

The UV sensitivity and dose-to-size of each resist is illustrated in Fig. 5.b. showing the dimensional shift of R_c, W_c, R_b and R_s values with respect to the dimensions of the UV mask and with respect to the irradiation energy density. On this graph, the phenomenon of overpolymerization is visible in the case of aPVZ10 and mPVZ10 but, on the other hand, it is clearly less intense for the boron-containing aPBVZ30-10 and mPBVZ30-10 photoresists. For resins with high UV sensitivity (*i.e.* aPVZ and mPVZ) a trend reversal may be observed e.g., the channel width W_c. To complete the microscopy observations, the influence of UV exposure on the topography of the micropatterns was evaluated by profilometry and is shown in Fig. SI 14. Overall, the profilometric representation of the samples confirmed our results: the width of the micropatterns increases with the UV exposure time and their values measured by profilometry are of the same order of magnitude as for

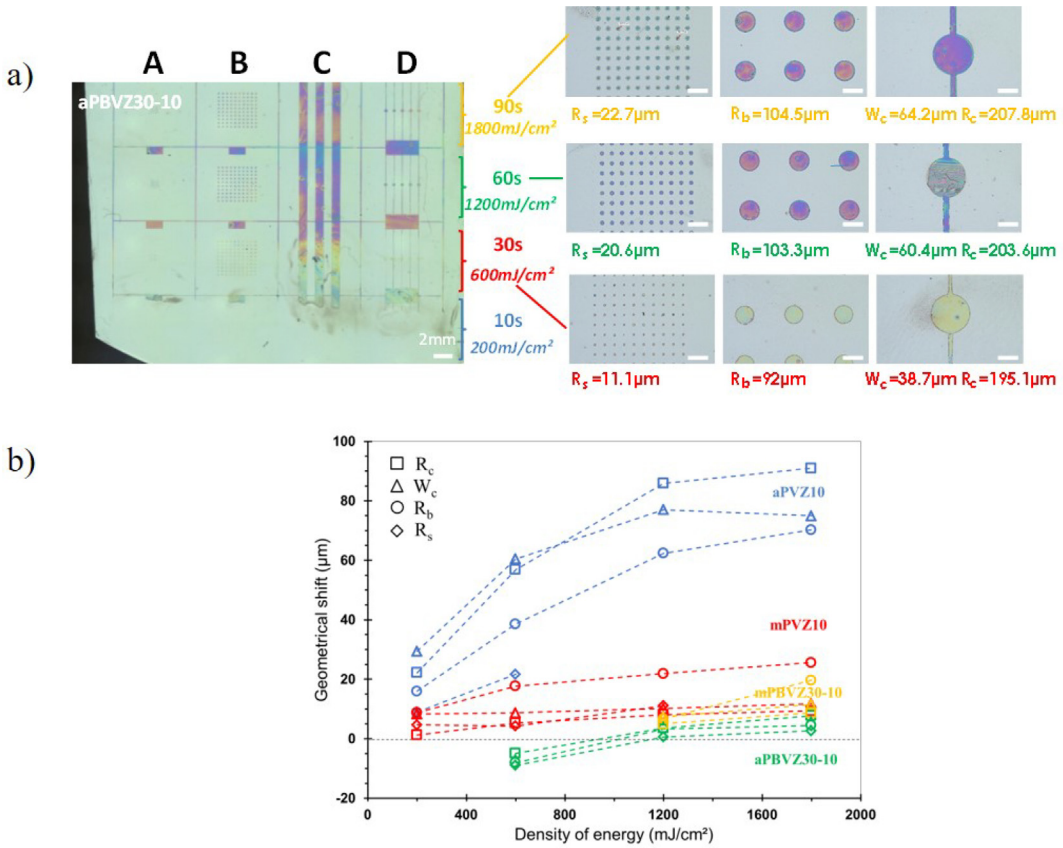

Fig. 4. a) Test of UV-dose for aPBZ30-10 photoresist; before pyrolysis (scale bar 200 200 µm) b) Geometrical shift on Rc, Wc, Rb and Rs dimensions against the irradiating density of energy. Measured on the UV crosslinked photoresist aPVZ10; mPVZ10; mPBVZ30-10 and aPBVZ30-10.

the microscopic observations. By comparing the micropatterns profiles, it is clear that the exposition time greatly influences the shape and the measured height. Regarding aPBVZ30-10 and mPBVZ30-10 profiles, their "wall-like shape" with vertical edges is quite similar and their height and width increase with exposure time. On the contrary, for aPVZ10 photoresists, as the channel's width increases its height decreases with the irradiation energy density. Moreover, the shape in the case of aPVZ10 observed for higher exposure changes from "wall-like" to "dome-like" shape. These changes in shape and height can be explained by two causes: (i) the increase in width was previously attributed to overpolymerization (see Fig. 5.a and b) (ii) the decrease in height could be associated with shrinkage occurring during photopolymerization of the resin.

3.2.1.2. After pyrolysis. The shrinkage evaluation occurring during pyrolysis was studied by profilometry (see Fig. 5). Usually, in the case of "channel-like" microstructure, the shrinkage that occurs during drying or after thermal treatment leads to a double-peak profile [54]. This shape is observable on the profiles shown in Fig. 5, in particular for aPBVZ30-10, mPBVZ30-10 and mPVZ10. Overall, it seems clear that the lateral shrinkage occurring during the heat treatment is very low regardless of the concerned photoresist. On the other hand, radial shrinkage is very important. It is consistent with the Griffith criterion discussed in the work of *Lange* [55]. Indeed the thickness plays a critical role in lithography process, due to the low thickness of the prepared micropatterns, the direction of shrinkage is almost entirely radial.

3.2.2. Surface properties

Both the top surface roughness and the thickness profile of micropatterns made of aPVZ10 and aPBVZ30-10 were studied by AFM. The AFM topographic profile presented in Fig. 6.a indicates that the aPVZ10 micropattern has an average thickness of ~ 250–300 nm and a height profile width of ~ 11 µm. The typical AFM topographic image presented in Fig. 6.b reveals that the SiBCN micropatterns have a root mean square (RMS) roughness surface of ~ 0.8 nm, and no traces of micro- or nano-cracks are detected. Note that (bright) small clusters of a few tens of nanometers can be distinguished and could be formed by gas release occurring during pyrolysis. For comparison, the AFM topographic profile as well as the top surface image of aPBVZ30-10 micropattern are also presented in Fig. 6.c and 6.d. The AFM topographic profiles show that the aPBVZ30-10 micropattern has an average thickness of ~ 110 nm and a height profile width of ~ 1 µm while a RMS roughness surface of ~ 2.9 nm was extracted from the AFM topographic view. For both samples, the AFM results are in agreement with the profilometry data discussed in the previous paragraph and the SEM observation displayed and discussed in supporting information (Fig. SI 15). Although the work was not performed in a clean room, we can notice that both the aPVZ 10 and aPBVZ30-10 micropatterns exhibit low RMS roughness surfaces (*i.e.* below 3 nm) which is an encouraging result as microfluidic requires smooth surfaces to ensure undisturbed fluid flow.

3.2.3. Mechanical properties

We evaluated the mechanical properties of the ceramic micropatterns using the nano-indentation technique. It is important to ensure that SiCN and SiBCN microstructures resulting from the pyrolysis of the photoresists exhibit Young's modulus values

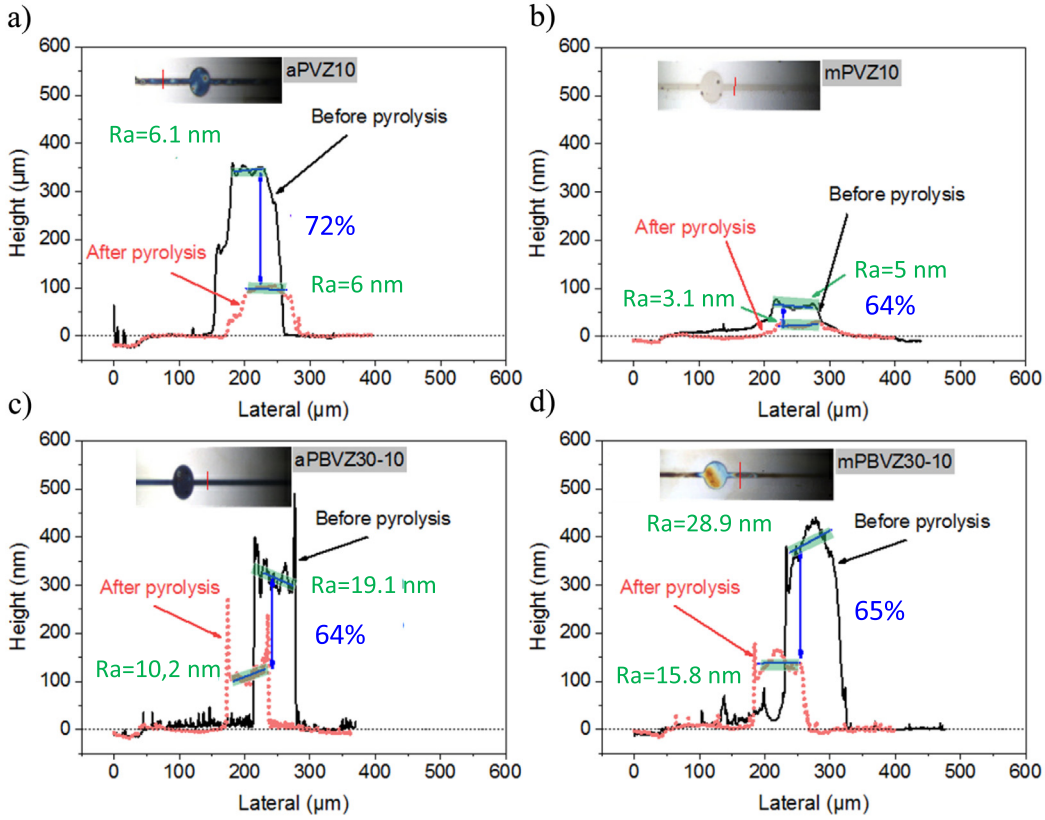

Fig. 5. Profilometry analysis of ceramic micropatterns derived from a) aPVZ10, b) mPVZ10, c) aPBVZ30-10 and d) mPBVZ30-10 photoresists.

compatible with the PDC materials. Fig. 7.a displays optical micrographs explaining the indentation area on aPVZ10 sample after pyrolysis at 1000 °C. Irisation phenomenon is observable on the sample and illustrates the inhomogeneity of the coating thickness, therefore indentation was carried out on distinct zones. Five indentations were performed in each area. The stiffness of the film was evaluated between 55 and 65 GPa which is similar to the Young's modulus value reported for analogous studies [35,36]. For example, the load–displacement curve displayed in Fig. 7.a was collected for one of the indentation regions; it confirms the brittle behavior of the microstructure with a Young modulus reaching 65 GPa. For comparison, a recently developed polymer based photoresist has an elastic modulus close to 3.2 GPa [58]. A comparative study was carried out on SiBCN micropattern derived from aPBVZ30-10. A greater homogeneity of the thickness was noticed for this sample, a simple set of four measurements is sufficient to collect a precise value of the Young's modulus. According to this result (Fig. 7.b), the introduction of boron in the Si—C—N matrix seems to decrease the mechanical properties of the film with a Young modulus of ~ 39 GPa, which is in agreement with the literature [21].

4. Conclusion

In this work, we describe a molecular design approach of photopatternable preceramic polymers precursors of SiBCN ceramics. For the first time, we prepared a tailor-made SiBCN polymer precursor by grafting UV-curable functions *i.e.* acrylate or methacrylate on the boron-containing polymer backbone, which turned the boron-containing polymer photo-responsive. Direct photolithography was then used to pattern the as-synthesized photoresists that convert after annealing to ceramic microstructures. Characterization of the photopolymers and the derived ceramics is systematically presented with emphasis on the correlation between the chemical composition and the photopolymerization behavior of the resists. Thin, crack-free non-oxide microstructures with Young's modulus as high as ~ 60 GPa were obtained. Overall, our study lay the groundwork for a rational approach towards the design and advanced patterning of highly stable SiBCN ceramic microparts. This two-step approach, combining precursor's chemistry with lithography, is versatile and could also be extended to other ceramics which composition and properties can be customized "on-demand" to control the quality and functionalities of the microstructures. Our investigations on designing complex quaternary ceramics could therefore bridge the gap between chemistry and engineering and benefit both fields. Finally, we also stress that this work will lay the ground for a rational approach towards not only microfabrication but also additive manufacturing by vat photopolymerization of SiBCN ceramics. Our rationally designed SiBCN polymer precursor has potential for other manufacturing strategies and in particular 3D printing. This underscores the versatility of our strategy for realizing complex designs, which are currently difficult to achieve using conventional top-down strategies.

CRediT authorship contribution statement

Quentin Hanniet: Investigation, Validation, Writing – original draft. **Eddy Petit:** Resources, Writing – review & editing. **Sylvie Calas-Etienne:** Resources, Investigation, Writing – review & editing. **Pascal Etienne:** Writing – review & editing. **Karim Aissou:** Writing – review & editing. **Christel Gervais:** Resources, Writing – review & editing. **Philippe Miele:** Resources, Writing – review & editing. **Benoit Charlot:** Resources, Methodology, Writing –

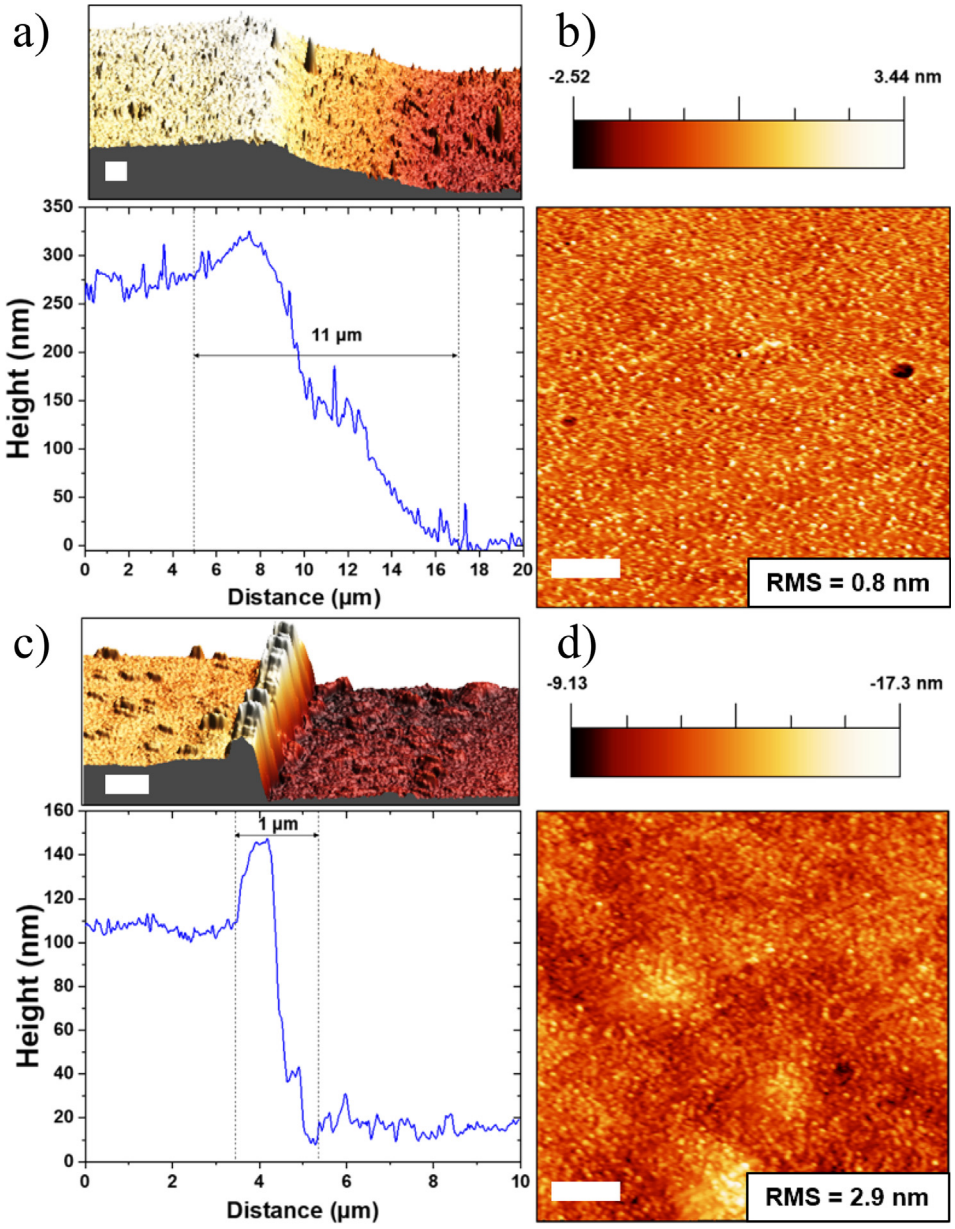

Fig. 6. a) 3D AFM topographic image and heights profile of aPVZ10, b) (3x3 µm) AFM topographic image of the top surface of aPVZ10, c) 3D AFM topographic image and heights profile of aPBVZ30-10 and d) (3x3 µm) AFM topographic image of the top surface of aPBVZ30-10. Scale bars: 500 nm.

review & editing. **Chrystelle Salameh:** Conceptualization, Methodology, Validation, Investigation, Resources, Data curation, Writing – review & editing, Visualization, Supervision, Project administration, Funding acquisition.

Data availability

Data will be made available on request.

Declaration of Competing Interest

The authors declare that they have no known competing financial interests or personal relationships that could have appeared to influence the work reported in this paper.

Acknowledgements

Chrystelle Salameh acknowledges financial supports from the French National Agency (ANR, JCJC program MONOME-ANR-20-CE08-0009), the CNRS Cellule Energie exploratory project PEPS (CeraMicroPac) and IEM Axe Energy project PAT (Solid CeraLique). Didier Cot is acknowledged for support with SEM.

Conflicts of interest

The authors declare that they have no known competing financial interests or personal relationships that could have appeared to influence the work reported in this paper.

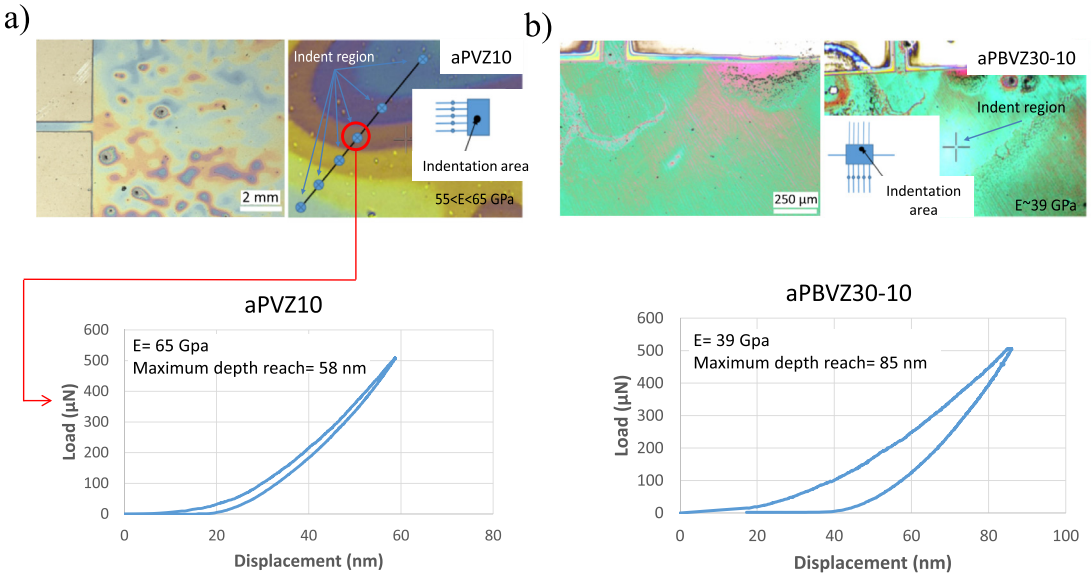

Fig. 7. Nanoindentation region and load–displacement curve associated with a) aPVZ10-derived SiCN and b) aPBVZ30-10-derived SiBCN.

Data availability

The raw/processed data required to reproduce these findings cannot be shared at this time due to technical or time limitations.

Appendix A. Supplementary data

Supplementary data to this article can be found online at https://doi.org/10.1016/j.matdes.2022.111234.

References

[1] M.C. McAlpine, R.S. Friedman, C.M. Lieber, Nanoimprint Lithography for Hybrid Plastic Electronics, Nano Lett. 3 (2003) 443–445, https://doi.org/10.1021/nl034031e.
[2] D. Pisignano, L. Persano, M.F. Raganato, P. Visconti, R. Cingolani, G. Barbarella, L. Favaretto, G. Gigli, Room-Temperature Nanoimprint Lithography of Non-thermoplastic Organic Films, Adv. Mater. 16 (2004) 525–529, https://doi.org/10.1002/adma.200305832.
[3] S. Chung, J.H. Lee, M.-W. Moon, J. Han, R.D. Kamm, Non-Lithographic Wrinkle Nanochannels for Protein Preconcentration, Adv. Mater. 20 (2008) 3011–3016, https://doi.org/10.1002/adma.200701715.
[4] S. Sathiamoorthy, K.J. Tiwari, G.R. Devi, M.S. Ramachandra Rao, P. Malar, Photoresist template fabrication and template assisted growth for surface patterning of technologically important Cu 2 ZnSnSe 4 thin films, Materials & Design. 127 (2017) 126–133, https://doi.org/10.1016/j.matdes.2017.04.055.
[5] B. Xue, Y. Zou, Y. Yang, A photochemical approach for preparing graphene and fabrication of SU-8/graphene composite conductive micropatterns, Materials & Design. 132 (2017) 505–511, https://doi.org/10.1016/j.matdes.2017.07.034.
[6] Z. Mehmood, I. Haneef, F. Udrea, Material selection for Micro-Electro-Mechanical-Systems (MEMS) using Ashby's approach, Materials & Design. 157 (2018) 412–430, https://doi.org/10.1016/j.matdes.2018.07.058.
[7] L.-A. Liew, W. Zhang, L. An, S. Shah, R. Luo, Y. Liu, T. Cross, M.L. Dunn, V. Bright, J.W. Daily, R. Raj, K. Anseth, Ceramic MEMS - New materials, innovative processing and future applications, American Ceramic Society Bulletin. 80 (2001) 25–30.
[8] L.-A. Liew, W. Zhang, V.M. Bright, L. An, M.L. Dunn, R. Raj, Fabrication of SiCN ceramic MEMS using injectable polymer-precursor technique, Sensors and Actuators A: Physical. 89 (2001) 64–70, https://doi.org/10.1016/S0924-4247(00)00545-8.
[9] N.R. Nagaiah, A.K. Sleiti, S. Rodriguez, J.S. Kapat, L. An, L. Chow, A novel design and analysis of a MEMS ceramic hot-wire anemometer for high temperature applications, Journal of Physics: Conference Series. 34 (2006) 277, https://doi.org/10.1088/1742-6596/34/1/046.
[10] N.R. Nagaiah, J.S. Kapat, L. An, L. Chow, Novel polymer derived ceramic-high temperature heat flux sensor for gas turbine environment, J. Phys.: Conf. Ser. 34 (2006) 458, https://doi.org/10.1088/1742-6596/34/1/075.
[11] C. Rossi, D. Estève, C. Mingués, Pyrotechnic actuator: a new generation of Si integrated actuator, Sensors and Actuators A: Physical. 74 (1999) 211–215, https://doi.org/10.1016/S0924-4247(98)00319-7.
[12] J.J. Licari, L.R. Enlow, Hybrid microcircuit technology handbook materials, processes, design, testing and production, Noyes [Orig.-Prod., Westwood, NJ, 1998. http://site.ebrary.com/id/10265840 (accessed February 1, 2022).
[13] M. Van Stappen, L.M. Stals, M. Kerkhofs, C. Quaeyhaegens, State of the art for the industrial use of ceramic PVD coatings, Surface and Coatings Technology. 74–75 (1995) 629–633, https://doi.org/10.1016/0257-8972(95)08296-4.
[14] N. Sharma, M. Hooda, S.K. Sharma, Synthesis and Characterization of LPCVD Polysilicon and Silicon Nitride Thin Films for MEMS Applications, Journal of Materials. 2014 (2014) e954618. https://doi.org/10.1155/2014/954618.
[15] Y. Liu, S. Peng, Y. Cui, X. Chang, C. Zhang, X. Huang, K. Han, M. Yu, Fabrication and properties of precursor-derived SiBN ternary ceramic fibers, Materials & Design. 128 (2017) 150–156, https://doi.org/10.1016/j.matdes.2017.05.018.
[16] H. Hur, Y. Jin Park, D.-H. Kim, J. Wan Ko, Material extrusion for ceramic additive manufacturing with polymer-free ceramic precursor binder, Materials & Design. 221 (2022) 110930. https://doi.org/10.1016/j.matdes.2022.110930.
[17] S. Vijayavenkataraman, L.Y. Kuan, W.F. Lu, 3D-printed ceramic triply periodic minimal surface structures for design of functionally graded bone implants, Materials & Design. 191 (2020), https://doi.org/10.1016/j.matdes.2020.108602 108602.
[18] G.-S. Chung, R. Maboudian, Bonding characteristics of 3C-SiC wafers with hydrofluoric acid for high-temperature MEMS applications, Sensors and Actuators A: Physical. 119 (2005) 599–604, https://doi.org/10.1016/j.sna.2004.10.004.
[19] K. Choy, Chemical vapour deposition of coatings, Progress in Materials Science. 48 (2003) 57–170, https://doi.org/10.1016/S0079-6425(01)00009-3.
[20] G. El Chawich, J. El Hayek, V. Rouessac, D. Cot, B. Rebière, R. Habchi, H. Garay, M. Bechelany, M. Zakhour, P. Miele, C. Salameh, Design and Manufacturing of Si-Based Non-Oxide Cellular Ceramic Structures through Indirect 3D Printing, Materials. 15 (2022) 471, https://doi.org/10.3390/ma15020471.
[21] P. Colombo, G. Mera, R. Riedel, G.D. Sorarù, Polymer-Derived Ceramics: 40 Years of Research and Innovation in Advanced Ceramics, Journal of the American Ceramic Society. 93 (2010) 1805–1837, https://doi.org/10.1111/j.1551-2916.2010.03876.x.
[22] J.C. McDonald, D.C. Duffy, J.R. Anderson, D.T. Chiu, H. Wu, O.J.A. Schueller, G.M. Whitesides, Fabrication of microfluidic systems in poly(dimethylsiloxane), ELECTROPHORESIS. 21 (2000) 27–40, https://doi.org/10.1002/(SICI)1522-2683(20000101)21:1<27::AID-ELPS27>3.0.CO;2-C.
[23] L.F. Thompson, C.G. Willson, M.J. Bowden, eds., Introduction to Microlithography: Theory, Materials, and Processing, AMERICAN CHEMICAL SOCIETY, WASHINGTON, D. C., 1983. https://doi.org/10.1021/bk-1983-0219.
[24] C.G. Willson, R.R. Dammel, A. Reiser, Photoresist materials: a historical perspective, in: Santa Clara, CA, USA, 1997: p. 38. https://doi.org/10.1117/12.275921.
[25] J.A. Rogers, R.G. Nuzzo, Recent progress in soft lithography, Materials Today. 8 (2005) 50–56, https://doi.org/10.1016/S1369-7021(05)00702-9.
[26] Y. Xia, G.M. Whitesides, Soft Lithography, Annual Review of Materials Science. 28 (1998) 153–184, https://doi.org/10.1146/annurev.matsci.28.1.153.
[27] Q.D. Nghiem, A. Asthana, I.-K. Sung, D.-P. Kim, Fabrication of porous SiC-based ceramic microchannels via pyrolysis of templated preceramic polymers, Journal of Materials Research. 21 (2006) 1543–1549, https://doi.org/10.1557/jmr.2006.0192.
[28] X. Liu, Y.-L. Li, F. Hou, Fabrication of SiOC Ceramic Microparts and Patterned Structures from Polysiloxanes via Liquid Cast and Pyrolysis, Journal of the

American Ceramic Society. 92 (2009) 49–53, https://doi.org/10.1111/j.1551-2916.2008.02849.x.
[29] E. Ionescu, S. Martinez Crespiera, M. Schlosser, R. Riedel, K. Flittner, H. F. Schlaak, P3.4 - Fabrication of Silicon Oxycarbide-Based Microcomponents via Photolithographic and Soft Lithography Approaches, (2013) 4 Pages, 379 KB. https://doi.org/10.5162/sensor2013/p3.4.
[30] H.-J. Lee, T.-H. Yoon, D.-P. Kim, Nano-sized patterns derived from a SiCN preceramic polymer: Fabrication and their characterization, Journal of Physics and Chemistry of Solids. 69 (2008) 2131–2136, https://doi.org/10.1016/j.jpcs.2008.01.018.
[31] D.-H. Lee, K.-H. Park, L.-Y. Hong, D.-P. Kim, SiCN ceramic patterns fabricated by soft lithography techniques, Sensors and Actuators A: Physical. 135 (2007) 895–901, https://doi.org/10.1016/j.sna.2006.09.003.
[32] S. Park, A. Böker, Ceramic nanowrinkles via a facile replication process, J. Mater. Chem. 21 (2011) 11734–11736, https://doi.org/10.1039/C1JM12007G.
[33] H. Yang, P. Deschatelets, S.T. Brittain, G.M. Whitesides, Fabrication of High Performance Ceramic Microstructures from a Polymeric Precursor Using Soft Lithography, Advanced Materials. 13 (2001) 54–58, https://doi.org/10.1002/1521-4095(200101)13:1<54::AID-ADMA54>3.0.CO;2-Y.
[34] M. Schulz, Polymer derived ceramics in MEMS/NEMS – a review on production processes and application, Advances in Applied Ceramics. 108 (2009) 454–460, https://doi.org/10.1179/174367609X422171.
[35] T. Anh Pham, P. Kim, M. Kwak, K.Y. Suh, D. Kim, Inorganic Polymer Photoresist for Direct Ceramic Patterning by Photolithography, Chemical Communications (Cambridge, England) 39 (2007) 4021–4023, https://doi.org/10.1039/b708480c.
[36] T.A. Pham, D.-P. Kim, T.-W. Lim, S.-H. Park, D.-Y. Yang, K.-S. Lee, Three-Dimensional SiCN Ceramic Microstructures via Nano-Stereolithography of Inorganic Polymer Photoresists, Advanced Functional Materials. 16 (2006) 1235–1241, https://doi.org/10.1002/adfm.200600009.
[37] J. Kong, X. Fan, G. Zhang, X. Xie, Q. Si, S. Wang, Synthesis and UV-curing behaviors of novel rapid UV-curable polyorganosilazanes, Polymer. 47 (2006) 1519–1525, https://doi.org/10.1016/j.polymer.2006.01.007.
[38] Y.-H. Li, X.-D. Li, D.-P. Kim, Acrylation of polyvinylsilazane with allyl bromide for an UV photosensitive inorganic polymer, Journal of Organometallic Chemistry. 692 (2007) 5303–5306, https://doi.org/10.1016/j.jorganchem.2007.08.016.
[39] Y.-H. Li, X.-D. Li, D.-P. Kim, Chemical development of preceramic polyvinylsilazane photoresist for ceramic patterning, J Electroceram. 23 (2-4) (2009) 133–136.
[40] Y.-H. Li, K.-D. Ahn, D.-P. Kim, Synthesis and properties of UV curable polyvinylsilazane as a precursor for micro-structuring, Polymers for Advanced Technologies. 26 (2015) 245–249, https://doi.org/10.1002/pat.3448.
[41] C.T. Nguyen, P.H. Hoang, J. Perumal, D.-P. Kim, An inorganic–organic diblock copolymer photoresist for direct mesoporous SiCN ceramic patterns via photolithography, Chemical Communications. 47 (2011) 3484, https://doi.org/10.1039/c0cc05836j.
[42] K.-W. Gyak, S. Jeon, L. Ha, S. Kim, J. Kim, K.-S. Lee, H. Choi, D.-P. Kim, Magnetically Actuated SiCN-Based Ceramic Microrobot for Guided Cell Delivery, Advanced Healthcare Materials. 8 (2019) 1900739, https://doi.org/10.1002/adhm.201900739.
[43] J. Schmidt, P. Colombo, Digital light processing of ceramic components from polysiloxanes, Journal of the European Ceramic Society. 38 (2018) 57–66, https://doi.org/10.1016/j.jeurceramsoc.2017.07.033.
[44] S. Park, D.-H. Lee, H.-I. Ryoo, T.-W. Lim, D.-Y. Yang, D.-P. Kim, Fabrication of three-dimensional SiC ceramic microstructures with near-zero shrinkage via dual crosslinking induced stereolithography, Chemical Communications. (2009) 4880–4882, https://doi.org/10.1039/B907923H.
[45] M. Zaheer, T. Schmalz, G. Motz, R. Kempe, Polymer derived non-oxide ceramics modified with late transition metals, Chemical Society Reviews. 41 (2012) 5102–5116, https://doi.org/10.1039/C2CS15326B.
[46] C. Salameh, S. Bernard, C. Gervais, F. Babonneau, A. Bruma, S. Malo, P. Miele, Chemistry of a series of aluminum-modified polysilazanes: Synthesis, pyrolysis behaviour and microstructural evolution, Journal of the European Ceramic Society. 39 (2019) 183–194, https://doi.org/10.1016/j.jeurceramsoc.2018.09.027.
[47] Q. Hanniet, M. Boussmen, J. Barés, V. Huon, I. Iatsunskyi, E. Coy, M. Bechelany, C. Gervais, D. Voiry, P. Miele, C. Salameh, Investigation of polymer-derived Si–(B)–C–N ceramic/reduced graphene oxide composite systems as active catalysts towards the hydrogen evolution reaction, Sci Rep. 10 (2020) 22003, https://doi.org/10.1038/s41598-020-78558-x.
[48] A. Viard, D. Fonblanc, M. Schmidt, A. Lale, C. Salameh, A. Soleilhavoup, M. Wynn, P. Champagne, S. Cerneaux, F. Babonneau, G. Chollon, F. Rossignol, C. Gervais, S. Bernard, Molecular Chemistry and Engineering of Boron-Modified Polyorganosilazanes as New Processable and Functional SiBCN Precursors, Chemistry – A, European Journal. 23 (2017) 9076–9090, https://doi.org/10.1002/chem.201700623.
[49] S. Sarkar, Z. Gan, L. An, L. Zhai, Structural Evolution of Polymer-Derived Amorphous SiBCN Ceramics at High Temperature, The Journal of Physical Chemistry C. 115 (2011) 24993–25000, https://doi.org/10.1021/jp203287h.
[50] A. Viard, L. Gottardo, D. Lopez-Ferber, A. Soleilhavoup, C. Salameh, S. Samal, Y. Gueguen, T. Rouxel, G. Motz, F. Babonneau, C. Gervais, S. Bernard, Molecular design of melt-spinnable co-polymers as Si–B–C–N fiber precursors, Dalton Transactions. 46 (2017) 13510–13523, https://doi.org/10.1039/C7DT02559A.
[51] A. Jalowiecki, J. Bill, F. Aldinger, J. Mayer, Interface characterization of nanosized B-doped Si3N4/SiC ceramics, Composites Part A: Applied Science and Manufacturing. 27 (1996) 717–721, https://doi.org/10.1016/1359-835X(96)00004-8.
[52] M. Christ, A. Zimmermann, A. Zern, M. Weinmann, F. Aldinger, An Improved Technique for Determining Hardness and Elastic Moduli using Load and Displacement Sensing Indentation Experiments, Journal of Materials Science. 36 (2001) 5767–5772, https://doi.org/10.1023/A:1012991618775.
[53] W.C. Oliver, G.M. Pharr, An improved technique for determining hardness and elastic modulus using load and displacement sensing indentation experiments, J. Mater. Res. 7 (1992) 1564–1583, https://doi.org/10.1557/JMR.1992.1564.
[54] C.R. Martin, I.A. Aksay, Topographical Evolution of Lead Zirconate Titanate (PZT) Thin Films Patterned by Micromolding in Capillaries, The Journal of Physical Chemistry B. 107 (2003) 4261–4268, https://doi.org/10.1021/jp034055+.
[55] F.F. Lange, Chemical Solution Routes to Single-Crystal Thin Films, Science. 273 (1996) 903–909, https://doi.org/10.1126/science.273.5277.903.
[56] P. Trefonas III, C.A. Mack, Exposure dose optimization for a positive resist containing polyfunctional photoactive compound, in: H. Ito (Ed.), San Jose, United States, 1991: pp. 117–131. https://doi.org/10.1117/12.46363.
[57] Y. Ding, Y. Xin, Q. Zhang, Y. Zou, Acrylic resins with oxetane pendant groups for free radical and cationic dual-curing photoresists, Materials & Design. 213 (2022), https://doi.org/10.1016/j.matdes.2021.110370 110370.
[58] N. Rohbeck, R. Ramachandramoorthy, D. Casari, P. Schürch, T.E.J. Edwards, L. Schilinsky, L. Philippe, J. Schwiedrzik, J. Michler, Effect of high strain rates and temperature on the micromechanical properties of 3D-printed polymer structures made by two-photon lithography, Materials & Design. 195 (2020), https://doi.org/10.1016/j.matdes.2020.108977 108977.